Perforin proteostasis is regulated through its C2 domain: supra-physiological cell death mediated by T431D-perforin

Amelia J Brennan [1], Ruby HP Law [2,3], Paul J Conroy [2,3], Tahereh Noori[1], Natalya Lukoyanova [4], Helen Saibil [4], Hideo Yagita[5], Annette Ciccone [6], Sandra Verschoor [6], James C Whisstock[2,3], Joseph A Trapani [6,7] and Ilia Voskoboinik [1,7].

[1] Killer Cell Biology Laboratory, Peter MacCallum Cancer Centre, East Melbourne, Australia.

[2] Department of Biochemistry and Molecular Biology, Monash University, Clayton, Melbourne, Australia.

[3] The ARC Centre of Excellence in Advanced Molecular Imaging, Monash University, Melbourne, Australia.

[4] Department of Crystallography/Biological Sciences, Institute of Structural and Molecular Biology, Birkbeck College, London, United Kingdom.

[5] Department of Immunology, Juntendo University School of Medicine, Tokyo 113-8421, Japan.

[6] Cancer Cell Death Laboratory, Peter MacCallum Cancer Centre, East Melbourne, Australia.

[7] Sir Peter MacCallum Department of Oncology, University of Melbourne, Melbourne, Australia.

Address correspondence to: Ilia Voskoboinik (ilia.voskoboinik@petermac.org) or Amelia Brennan (amelia.brennan@petermac.org)

Peter MacCallum Cancer Centre,

305 Grattan Street,

Melbourne,

VIC 3000

Australia

ph.: (+61) 424 860 139

Running Title: Generation of super-perforin

Abstract

The pore forming, Ca^{2+}-dependent protein, perforin, is essential for the function of cytotoxic lymphocytes, which are at the frontline of immune defence against pathogens and cancer. Perforin is a glycoprotein stored in the secretory granules prior to release into the immune synapse. Congenital perforin deficiency causes fatal immune dysregulation, and is associated with various haematological malignancies. At least 50% of pathological missense mutations in perforin result in protein misfolding and retention in the endoplasmic reticulum. However, the regulation of perforin proteostasis remains unexplored. Using a variety of biochemical assays that assess protein stability and acquisition of complex glycosylation, we demonstrated that the binding of Ca^{2+} to the C2 domain stabilizes perforin and regulates its export from the endoplasmic reticulum to the secretory granules. Since perforin is a thermo-labile protein, we hypothesized that by altering its C2 domain it may be possible to improve protein stability. Based on the X-ray crystal structure of the perforin C2 domain, we designed a mutation (T431D) in the Ca^{2+} binding loop. Mutant perforin displayed dramatically enhanced thermal stability and lytic function, despite its trafficking from the endoplasmic reticulum remaining unchanged. Furthermore, by introducing the T431D mutation into A90V-perforin, a pathogenic mutation, which results in protein misfolding, we corrected the A90V folding defect and completely restored perforin's cytotoxic function. These results revealed an unexpected role for the Ca^{2+}-dependent C2 domain in maintaining perforin proteostasis and demonstrated the possibility of designing perforin with supra-physiological cytotoxic function through stabilization of the C2 domain.

Introduction

Cytotoxic T lymphocytes and natural killer cells recognize and destroy virus-infected and transformed cancerous cells through the exquisitely regulated secretory granule exocytosis pathway [1]. Central to this mechanism is the pore-forming effector protein, Prf1 (Prf1), which is stored in cytotoxic secretory granules and co-secreted with the pro-apoptotic serine proteases, granzymes, into the immune-synapse formed between a cytotoxic lymphocyte and target cell [2]. The high concentration of extracellular Ca^{2+} (>1mM) promotes binding of the Prf1 through its C2 domain to the target cell [3] via a single localized conformational change, which repositions 4 key hydrophobic residues and promotes anchoring of Prf1 to the plasma membrane [4]. Once bound, the neutral pH of the synapse facilitates Prf1 oligomerisation [5] into ring and arc-shaped pores [6, 7], which are required for the diffusion of granzymes into the cytoplasm of the target cell to initiate apoptosis [8]. Prf1 therefore sits at the apex of the signaling cascade that triggers apoptotic target cell death and immune defense by cytotoxic lymphocytes.

The loss of perforin function due to bi-allelic mutations in the *PRF1* gene leads to a severe and often fatal form of immune dysregulation, familial haemophagocytic lymphohistiocytosis (FHL) [9]. If at least one of the affected alleles harbors a missense, hypomorphic mutation in *PRF1*, FHL may be delayed until adolescence or early adulthood, and there is also a high (up to 50%) risk of a haematological malignancy [10, 11]. A significant proportion of these missense mutations lead to perforin misfolding and retention in the endoplasmic reticulum (ER) [12]. Failure to traffic to the secretory granules results in failure of perforin secretion into the immune synapse and the loss of cytotoxic lymphocyte function. Similar to other protein misfolding diseases [13], perforin may partly recover its folding at permissive temperatures (for example, *in vitro* culture of cytotoxic lymphocytes at 30°C), with restoration of protein trafficking and cytotoxicity [12]. However, recovery of function is typically incomplete and less likely with mutations associated with poor clinical outcomes. Over 30 of the reported pathogenic missense mutations in *PRF1* map to the C2 domain, consistent with an essential role of that domain in perforin function; these mutations often result in perforin misfolding.

The C2 domain of perforin can coordinate up to five Ca^{2+} ions, including two high-affinity sites II and V [3]. Binding of Ca^{2+} to these two sites alone is not sufficient for membrane binding. In contrast, sites, I, III and IV bind Ca^{2+} at low affinity and are responsible for a conformational rearrangement of four conserved hydrophobic residues that are essential for perforin binding to the phospholipid bilayer [3]. The ER maintains an ionic Ca^{2+} concentration sufficiently high (500-

700μM) for Ca^{2+} binding and has neutral pH, and is the only intracellular compartment with an environment that may support perforin lysis. Indeed, we recently discovered that rapid export of perforin from the ER [14] and N-glycosylation close to the carboxy-terminus [15] are essential for protecting cytotoxic lymphocytes from their own endogenous perforin. As evidence, we showed that non-conservative mutations in a cryptic trafficking motif at the extreme C-terminus of perforin caused its retention in the ER and death of the killer cell; however introducing an additional mutation within the C2 domain to prevent Ca^{2+} binding restored cell viability without reversing the defect in trafficking. These observations clearly indicated that Ca^{2+} binds to the perforin C2 domain in the ER, but this does not compromise the viability or the effector function of the host cells. Intriguingly, it was recently found that physiological Ca^{2+} concentrations could stabilise perforin through the C2 domain [8], suggesting a role for Ca^{2+}/C2 domain interaction beyond the regulation of perforin binding to the target cell membrane following exocytosis.

In this study, we discovered that Ca^{2+}-dependent stabilisation of perforin through the C2 domain in the ER is required for its folding and the delivery to the secretory granules. Unexpectedly, we also identified a novel Ca^{2+} stabilizing mutation in the C2 domain that improved the kinetics of perforin pore formation and also enhanced its cytotoxicity to be greater than WT perforin; remarkably, it was also able to compensate for the folding and trafficking defect of a common disease-causing mutation, A90V.

Results

Ca^{2+} binding to the C2 domain of perforin in the ER is required for its folding and trafficking.

We recently demonstrated that perforin is a thermodynamically labile protein, which acquired a more stable conformation at physiological Ca^{2+} concentrations; this effect of Ca^{2+} was abrogated by mutations in the C2 domain [4, 8]. Given the high concentration of Ca^{2+} in the ER and the demonstrated ability of perforin to bind Ca^{2+} there [14], we hypothesised that Ca^{2+} binding to the C2 domain may play an important, previously unappreciated, role in perforin folding and export from the ER.

First, we substituted Ca^{2+}-binding aspartate residues, D429 and D483, each of which is essential for Ca^{2+} binding and perforin function [6, 16] and located within distinct Ca^{2+}-binding regions CBR1 and CBR2, respectively, with alanine (D429A and D483A) (Supplementary Figure 1) [6, 16]). These mutations completely abrogated perforin membrane binding and pore forming activity [16]. As perforin traffics from the ER through the Golgi compartment, N-linked, high mannose glycans attached at residues N204, N375 and N548 progressively undergo complex glycosylation. Accordingly, perforin that is retained in the ER lacks complex glycans and remains sensitive to endoglycosidase H (EndoH) [14]. We therefore assessed the EndoH resistance of WT and mutated perforins to determine their capacity to exit the ER.

Even though the expression levels of D429A and D483A were no different from WT, each demonstrated greater EndoH sensitivity than WT perforin (Figure 1A), indicating impaired export from the ER. In addition, simultaneously introducing both Ca^{2+} binding site mutations (D429A and D483A) did not further increase EndoH sensitivity, suggesting that failure to bind Ca^{2+} was sufficient to impair the export of the protein (Figure 1A). To further test the role of Ca^{2+} binding in conferring exit from the ER, we mutated D491 (D491A), a Ca^{2+}-binding residue located in CBR3. Previous studies have revealed that a mutation at this position does not abrogate Ca^{2+}-dependent membrane binding and pore formation at physiological concentrations of Ca^{2+} [16]. In contrast to D429A and D483A, D491A remained similarly resistant to EndoH as WT-perforin (Figure 1A).

Previously, we identified four hydrophobic residues (W427, Y430, Y486 and W488) that are key for interaction of the membrane proximal part of the C2 domain with the lipid membrane [4]. Mutation of these residues does not impact on Ca^{2+} binding [3, 4]. Accordingly, mutation of these four residues (W427A/Y430A/Y486A/W488A) did not impair mutant perforin export from the ER (Figure 1B). Taken together, these data suggest that it is the ability of the perforin C2 domain

to bind Ca^{2+}, rather than the interaction with the ER membranes *per se*, which influenced perforin export.

In humans, hypomorphic perforin missense mutations that destabilize folding but retain partial function are commonly associated with haematological cancer in childhood or adolescence and/or atypical or delayed presentation with FHL [12, 17]. These mutants are invariably retained in the ER and poorly exported to the secretory granules [12]. By far the most common mutation of this type is the A91V variant (mouse homologue A90V; Figure 1C); this allele is carried in the heterozygous state by 8-9% of Caucasians. A91V homozygocity is strongly associated with leukemia/lymphoma, systemic inflammatory disorders and atypical FHL [2]. As with human A91V [18, 19, 20], mouse A90V was partially misfolded and had a mild trafficking defect [20, 21]. To determine whether Ca^{2+} binding to perforin in the ER contributes to the stability of the A90V mutant, we combined A90V with mutations in critical Ca^{2+}-binding residues in the C2 domain described above, A90V/D429A, A90V/D483A and A90V/D491A. We found that the loss of Ca^{2+} binding (A90V/D429A or A90V/D483A) dramatically affected perforin stability and trafficking from the ER (Figure 1D). Indeed, the Endo H sensitivity of the double mutants exceeded the sum of A90V and Ca^{2+} binding mutants alone (A90V+D429A and A90V+D483A; Figure 1E and 1F *dotted lines*). Protein expression levels were also significantly reduced in comparison to WT-perforin. By contrast, mutation of the non-essential Ca^{2+}-binding residue D491A (A90V/D491A), did not further increase the EndoH sensitivity of A90V (Figure 1G), indicating that the misfolding defect of A90V/C2 domain double mutants was directly associated with loss of Ca^{2+} binding at the C2 domain. Taken together, our results demonstrated that Ca^{2+} binding to the perforin C2 domain in the ER is required for stable folding and subsequent export of perforin from the ER.

The folding and trafficking of A90V are rescued by Ca^{2+}-dependent stabilisation through the perforin C2 domain.

The C2 domain of perforin differs from most others in that the overall affinity for Ca^{2+} is low. Unlike other C2 domains that avidly bind Ca^{2+} at low μM or even sub-μM concentrations, perforin becomes functional only at neutral pH and when free Ca^{2+} levels exceed 250μM, a concentration found only in extracellular milieu (for instance, in the immunological synapse) or in the ER of intact cells.

Previously we have used NMR-based approaches, together with mutagenesis and crystallography, to demonstrate that the canonical Ca^{2+}-binding site III has the weakest affinity of all five Ca^{2+}-binding sites and is only filled at high concentrations of Ca^{2+} [3]. These findings are consistent with our data revealing that CBR-1 must undergo significant conformational change in order to bring the key residues D429 and D435 into position to bind Ca^{2+}. The rearrangement of CBR-1 further re-positions the four essential hydrophobic residues such that W427 and Y430 are in close proximity to Y486 and W488. Together these four hydrophobic residues are thus positioned to interact with the plasma membrane [4, 6].

We have previously suggested that the conformational change within CBR-1 is likely driven through electrostatic attraction to Ca^{2+} ions already bound at the high affinity sites I and II (since D429 also interacts with the site I and II and D435 interacts with site II). Based on these data, we reasoned that introduction of additional negatively charged residues into CBR1 may facilitate conformational changes within CBR1 through provision of additional short or longer range electrostatic interactions with bound Ca^{2+} ions in site I and II. Accordingly, and using X-ray crystal structures that we had previously solved as a guide [3, 6], we identified T431 as one potential site to introduce a negatively charged residue into CBR1 and generated the mutation T431D.

Previously, we showed that the thermal stability of perforin is dramatically increased in the presence of Ca^{2+} [8]. We therefore compared the thermal stability of the T431D variant to that of wild type perforin and found that the T431D substitution (Figure 2A) caused a dramatic increase in melting temperature at physiologically relevant concentrations of Ca^{2+}. Similar to WT, T431D-perforin stabilisation was Ca^{2+}-dependent, as simultaneously mutating the key Ca^{2+}-binding residue D429 (D429A/T431D double mutant) prevented this change (Figure 2A). Taken together, these data suggested that as predicted, the mutation was in some way facilitating Ca^{2+} binding.

As discussed, we originally reasoned that the T431D variant may either interact directly with one of the bound Ca^{2+} ions or alternatively may facilitate conformational change in CBR1. To discriminate between these possibilities we determined the apo- and Ca^{2+}-bound structures of a perforin C2 domain variant that contains the T431D mutation (mutant generated on the W427A/Y430A/Y486A/W488A background [3, 4]) (Figure 3). In the absence of Ca^{2+}, T431 is mobile and missing from the final model, whereas D431 is clear in the electron density (Figure 3A). In the presence of added Ca^{2+} however the Ca^{2+} ions in sites I, II and III are conventionally coordinated by the same residues as in wild type protein, and the T431D position does not

directly interact with Ca^{2+}. These data thus favour the idea that the T431D variant instead facilitates conformational change in CBR1, for example, through the provision of additional potential for long-range electrostatic interactions.

As we had shown Ca^{2+} binding in the ER regulates perforin folding and trafficking through stabilisation of its C2 domain, we hypothesized that T431D may potentially compensate for the misfolded phenotype of the A90V mutant. Due to folding defects of A90V, we were unable to produce sufficient amounts of the protein to assess its melting temperature, but we found that engineering the T431D mutation onto the backbone of A90V perforin (A90V/T431D) resulted in greater thermal stability than WT perforin (Figure 2A), and both T431D and A90V/T431D had a wild type level of cytotoxic activity (Figure 2B). Furthermore, in transiently transfected RBL cells, T431D improved EndoH sensitivity of A90V to the WT level (Figure 2C), suggesting that under steady-state conditions both folding and trafficking of A90V were restored. This process remained dependent on essential Ca^{2+}-binding residue/s of the C2 domain, as further addition of the D429A mutation (A90V/D429A/T431D) destabilised the protein and completely abrogated trafficking improvements provided by T431D (Figure 2D). Furthermore, the D429A/T431D mutant was as sensitive to EndoH as the single D429A mutant, indicating once again that Ca^{2+} binding to the C2 domain of perforin in the ER was essential for the stabilizing properties of T431D (Figure 2D). From these results, we concluded that Ca^{2+}-dependent stabilisation of the C2 domain in the ER is important for perforin folding, and subsequent trafficking to the secretory granules.

T431D-Prf1 has supra-physiological function.

Similar to the ER, the synaptic cleft has neutral pH and high concentration of free Ca^{2+} (>1mM). We therefore investigated whether enhanced stabilisation of T431D-perforin also affected its lytic function. Using purified recombinant WT and T431D proteins, we found no significant difference in their ability to bind to membranes (Figure 4A), pore-size/geometry by negative stain EM (Figure 4B) or to synergise with granzyme B to induce target cell apoptosis (Figure 4C). However, target cell lysis at 1 mM Ca^{2+} was twice as fast with T431D-perforin as with WT ($p<0.0005$) (Figure 4D). Interestingly, at sub-physiological concentrations of Ca^{2+} (<0.5mM), both T431D and A90V/T431D had relatively lower cytotoxic activity than WT (Figure 4E). Speculatively, this may be due to the loss of CaIV, which is coordinated by D491 (Figure 3).

Next, we investigated the effect of the T431D mutation on perforin cytotoxicity in the context of an immune synapse using a standard RBL ^{51}Cr release cytotoxicity assay [16]. The results were surprising: T431D-expressing RBL cells had >5-fold superior cytotoxicity in comparison to killer cells expressing WT perforin (Figure 5A), in that over 5-times fewer killer cells expressing T431D-perforin were required to produce an equivalent level of ^{51}Cr release (cell death). We also considered the possibility that overexpression of perforin in this experiment would potentially result in saturation of the cell death readout. Since perforin cDNA was cloned into pIRES-eGFP vector and transiently transfected into RBL effector cells, we sorted high and low perforin-expressing cells (based on eGFP fluorescence intensity) and assessed their cytotoxic activity separately. The cells expressing relatively low levels of T431D had >10-fold greater cytotoxicity than the cells expressing an equivalent amount of WT perforin (Figure 5B). This was not due to an increased affinity of the C2 domain for Ca^{2+}, as T431D was only cytotoxic at physiologically relevant concentrations of Ca^{2+}, and only displayed augmented cytotoxicity within the range of Ca^{2+} concentrations that corresponded with enhanced stability (Figure 5C).

Finally, we investigated whether improved folding or trafficking through Ca^{2+}-dependent stabilisation could also rescue A90V function. We found that this was indeed so: A90V/T431D cytotoxicity was significantly improved, above that of WT perforin (Figure 5D), which was likely due to a combination of improved folding (Figure 2A-C) and more rapid pore-formation (Figure 4D). To determine whether T431D facilitated trafficking of the A90V mutant, we assessed the rate of perforin export from the endoplasmic reticulum. Thus RBL cells were transiently transfected with perforin variants, and the rate of acquisition of complex glycosylation (EndoH resistance) over 90-240 minutes was a measure of perforin export from the ER and processing in the Golgi. The experiment demonstrated that the rate of trafficking of T431D was slightly higher than that of WT, but it did not improve the rate of A90V export from the endoplasmic reticulum (Figure 5E).

Overall, the results of this study demonstrate that Ca^{2+}-dependent stabilization of perforin through the C2 domain is required for its folding, function and proteostasis in general.

Discussion

The current study uncovered a novel and critical role for the C2 domain in maintaining Prf1 proteostasis. This was demonstrated using a dual approach, where we first improved and then abrogated Ca^{2+} binding to the C2 domain of Prf1. Remarkably, by engineering a new Ca^{2+}-stabilising mutation in the C2 domain of Prf1 (T431D), we produced a "super-Prf1", which had significantly higher cytotoxic activity than wild-type perforin. In addition, this mutant stabilized and rescued the delivery of a partially misfolded, common pathological mutant, A90V, to the secretory granules. In a reciprocal series of experiments, the abrogation of C2 domain function through mutation of critical Ca^{2+} binding aspartate residues resulted in a significant decrease in the delivery of A90V Prf1 to the secretory granules. Given that A90V is not part of the C2 domain, and its location is approximately 120Å away from the Ca^{2+}-binding regions [6], it appeared that Ca^{2+}-dependent stabilisation of the C2 domain was critical for the efficient folding and export of Prf1 from the ER. It is unclear why T431D-perforin enhances the stability and function of perforin, but the X-ray crystal structure suggests that this may be due to additional long-range electrostatic interactions within the C2 domain. Interestingly, we found that T431D had reduced cytotoxic activity at sub-physiological Ca^{2+} concentrations and that under our crystallization conditions it was missing one Ca^{2+} (CaIV) that was coordinated by D491. We are led to speculate that there may be a link between the two phenomena, as we showed previously that the D491A mutation had no effect on perforin function at physiological concentrations of Ca^{2+}, but the activity of the mutant was impaired at low (non-physiological) Ca^{2+} levels [16].

An increase in Prf1 stability through Ca^{2+} binding to the C2 domain also provided an oligomerisation advantage, whereby T431D could lyse cells at a faster rate than WT Prf1 to confer both augmented cytotoxicity and recovery of oligomerisation deficiencies. These results suggest that the more stable T431D Prf1 may be 'primed' for more efficient oligomerisation and, potentially, pore formation. This concept is supported by previous studies, which have reported that WT Prf1 becomes significantly more stable under conditions that favour Prf1 pore formation within the immunological synapse [4, 8]. Taken together, it appears that in addition to Ca^{2+}-dependent membrane binding [16], stabilisation of the C2 domain of WT Prf1 may be a previously unrecognized step required for pore formation.

The C2 domain of Prf1 is unique, with a relatively low affinity for Ca^{2+} in comparison with intracellular C2 domain proteins, which respond to submicromolar fluctuations in Ca^{2+} concentrations in order to become activated. Although the neutral pH and high concentration of

Ca^{2+} in the ER create a favorable environment for perforin lethal pore-forming activity, cytotoxic lymphocytes can rapidly export it through the Golgi to the acidic secretory granules [14]. In addition, the C-terminal glycosylation protects the cell from perforin toxicity within the endoplasmic reticulum [15]. The results of our study indicate that, paradoxically, the high level of Ca^{2+} in the ER promotes Prf1 stabilisation, which is necessary for efficient protein folding and trafficking. Unlike high affinity calcium binding sites II and V, which are likely to be constitutively occupied, low affinity Ca^{2+} binding sites I, III and IV act as a chemical sensor that only responds to high Ca^{2+} concentrations [4]. Once the protein has been folded and exported from the ER, it likely becomes functionally inert in the low Ca^{2+} environment of the Golgi and acidic pH of the secretory granules, where it is unable to oligomerise and insert into the membrane [8]. Overall, Ca^{2+} binding to the C2 domain plays a critical role in the proteostasis of Prf1, which requires a precise balance between Ca^{2+} and membrane binding, folding in the ER, export to the Golgi, and cytotoxic lymphocyte toxicity.

It is well established that disease-causing Prf1 mutations are the result of protein misfolding in the ER [12]. Our discovery that Prf1 folding in the ER is Ca^{2+}-dependent provides a rationale for the development and application of specific drug therapies for FHL caused by Prf1 deficiency. Patients with late-onset FHL2 often require aggressive cytotoxic drug therapy in order to treat the disease prior to bone marrow transplantation. Alternative therapies that modify the proteostasis network through a post-translational mechanism [21, 22] are significantly less aggressive and may provide a more suitable alternative to initial treatment. Such an approach would facilitate targeting of Prf1-expressing lymphocytes without damaging other cell types, and will be the focus of ongoing studies.

Materials and Methods

Expression and Binding of Recombinant perforin.

Mouse perforin mutants were expressed and purified using a baculovirus expression system as previously described [23]. Lytic activity were assessed using sheep erythrocytes (SRBC), and cell death resulting from the synergistic effects of perforin and granzyme B (GzmB) was assessed by ^{51}Cr release assays [24]. Membrane binding was assessed by incubating perforin and SRBCs in 10mM Hepes, 150mM NaCl, pH 7 with or without 1mM Ca^{2+} at 4C for 15 min, followed by 4 subsequent washes in Ca^{2+}-free buffer. The thermal stability of purified recombinant mouse WT and mutant perforin was assessed by unfolding temperature analysis using SYPRO Orange [4].

Transient Transfection of Cell Lines and Cytotoxicity Assays

Rat Basophil Leukemia cells RBL-2H3 (RBL) and Jurkat human T leukemia target cells were maintained in culture as previously described [23]. Point mutations in mouse WT perforin cDNA were generated using the QuikChange site-directed mutagenesis system and cloned into the pIRES-EGFP expression plasmid (Biosciences Clonech). The WT and mutant perforin plasmids were transiently transfected into RBL cells, which were sorted by flow cytometry for equal mean GFP fluorescence 24 hr later, with subsequent assessment of cytotoxic activity in ^{51}Cr release assays with Jurkat T cells [23]. Perforin expressing RBL cells sorted by flow cytometry for equal mean GFP fluorescence were also used for Western Immunoblot (see below).

Electrophoresis and Immunoblotting

Whole cell lysates, SRBC membranes and purified recombinant mouse perforin were prepared in NP40 lysis buffer (250 mM NaCl, 25 mM HEPES, 2.5 mM EDTA, 1% [v/v] NP-40, supplemented with protease inhibitors cocktail (Roche Life Sciences)). EndoH and PNGaseF glycosidase treatment was conducted according to the manufacturer's instructions (New England Biolabs). Protein lysates were separated on 4-12% Nu-Page Bis-Tris gradient gels (Invitrogen) and immunoblotted with rat anti-perforin mAb P1-8 (provided by Kyowa Kirin) followed by secondary HRP-linked anti-rat antibody. The loading control used for cell lysates was mouse anti-human actin mAb (Sigma) followed by secondary HRP-linked anti-mouse Ig (Dako). Signals were amplified by chemiluminescence and detected on X-ray film (GE Healthcare). ImageJ software (ImageJ 1.475v, NIH) was used for quantitative densitometry.

Negative stain electron microscopy sample preparation.

Purified recombinant WT and T431D perforin pores were formed on DMPC/cholesterol lipid monolayers as described [6]. Images were collected on a Gatan 4k X 4k CCD camera (15µm per pixel) on a Tecnai F20 microscope (FEI) at 200keV and 67,000X magnification.

Crystallography.

Recombinant perforin C2 domains (residues 410-535) were expressed and purified from E coli as described before [3]. A mutant form, which carries four amino acid substitutions (W427A/Y430A/Y486A/W488A, C2_T431) was used for the current studies to generate C2_D431. C2_T431D was crystallised in 0.2M Ammonium iodide, 20% PEG 3350 in the absence of added Ca^{2+}, or in 0.1 M MgCl2, 0.1 M Na-HEPES pH7.5 and 10% w/v PEG 4000 in the presence of 1mM Ca^{2+} (Table 1). The crystals were flash-cooled in liquid nitrogen using 25% (v/v) glycerol as the cryoprotectant. Data sets were collected at the Australian Synchrotron MX2 beamline at 100K. The data were merged and processed using XDS [25], POINTLESS [26] and SCALA [27] or AIMLESS [28]. Five per cent of the data set was flagged as a validation set for calculation of the Rfree. Molecular replacement (MR) was carried out using wild-type perforin structure 3NSJ as a search probe [29] One molecule was found per asymmetric unit cell and an initial model was generated using PHASER. Model building was performed using COOT [30] and refinement was performed using BUSTER (Cambridge, United Kingdom: Global Phasing Ltd). Crystallographic and structural analysis was performed using the CCP4 suite [27] unless otherwise specified. The figures were generated using MacPYMOL (The PyMOL Molecular Graphics System, Version 1.2r3pre, Schrödinger, LLC.) and the structural validation was performed using MolProbity [31]. All atomic coordinates and structural factors were deposited in the PDB under codes 5UG6 (in the absence of Ca^{2+}) and 5UG7 (in the presence of Ca^{2+}).

Statistical Analysis

The statistical analyses used were: paired t-test (when comparing two groups); or one-way ANOVA with Tukey's post-hoc analysis (when comparing more than two groups). The application of each test is indicated in the figure legends. A non-linear regression analysis was applied to all SRBC lysis assays and ^{51}Cr release killing assays for clarity.

Conflict of interests: Authors declare that they have no conflict of interests.

Acknowledgements

This work was supported by project and program grants from the National Health and Medical Research Council of Australia (to I.V., J.C.W. and J.A.T.), and Wellcome Trust equipment grant 079605 to H. Saibil. I.V. and J.C.W. are supported by a National Health and Medical Research Council of Australia Fellowships. We thank Colin House and Conor Kearney for critical reading of the manuscript, and Mr. Samuel J. Redmond for his technical assistance.

References

1. de Saint Basile G, Ménasché G, Fischer A. Molecular mechanisms of biogenesis and exocytosis of cytotoxic granules. *Nat Rev Immunol* 2010, **10:** 568-579.

2. Voskoboinik I, Whisstock JC, Trapani JA. Perforin and granzymes: function, dysfunction and human pathology. *Nat Rev Immunol* 2015, **15**(6): 388-400.

3. Yagi H, Conroy PJ, Leung EW, Law RH, Trapani JA, Voskoboinik I, *et al.* Structural Basis for Ca2+-mediated Interaction of the Perforin C2 Domain with Lipid Membranes. *J Biol Chem* 2015, **290**(42): 25213-25226.

4. Traore DA, Brennan AJ, Law RH, Dogovski C, Perugini MA, Lukoyanova N, *et al.* Defining the interaction of perforin with calcium and the phospholipid membrane. *The Biochemical journal* 2013, **456**(3): 323-335.

5. Leung C, Hodel AW, Brennan AJ, Lukoyanova N, Tran S, House CM, *et al.* Real-time visualization of perforin nanopore assembly. *Nat Nanotechnol* 2017, **12**(5): 467-473.

6. Law RH, Lukoyanova N, Voskoboinik I, Caradoc-Davies TT, Baran K, Dunstone MA, *et al.* The structural basis for membrane binding and pore formation by lymphocyte perforin. *Nature* 2010, **468**(7322): 447-451.

7. Metkar SS, Marchioretto M, Antonini V, Lunelli L, Wang B, Gilbert RJ, *et al.* Perforin oligomers form arcs in cellular membranes: a locus for intracellular delivery of granzymes. *Cell death and differentiation* 2015, **22**(1): 74-85.

8. Lopez JA, Susanto O, Jenkins MR, Lukoyanova N, Sutton VR, Law RH, *et al.* Perforin forms transient pores on the target cell plasma membrane to facilitate rapid access of granzymes during killer cell attack. *Blood* 2013, **121**(14): 2659-2668.

9. Janka GE. Familial and acquired hemophagocytic lymphohistiocytosis. *Annu Rev Med* 2012, **63:** 233-246.

10. Voskoboinik I, Smyth MJ, Trapani JA. Perforin-mediated target-cell death and immune homeostasis. *Nat Rev Immunol* 2006, **6**(12): 940-952.

11. Lofstedt A, Chiang SC, Onelov E, Bryceson YT, Meeths M, Henter JI. Cancer risk in relatives of patients with a primary disorder of lymphocyte cytotoxicity: a retrospective cohort study. *Lancet Haematol* 2015, **2**(12): e536-542.

12. Chia J, Yeo KP, Whisstock JC, Dunstone MA, Trapani JA, Voskoboinik I. Temperature sensitivity of human perforin mutants unmasks subtotal loss of cytotoxicity, delayed FHL, and a predisposition to cancer. *Proceedings of the National Academy of Sciences of the United States of America* 2009, **106**(24): 9809-9814.

13. Wiseman RL, Powers ET, Buxbaum JN, Kelly JW, Balch WE. An adaptable standard for protein export from the endoplasmic reticulum. *Cell* 2007, **131**(4): 809-821.

14. Brennan AJ, Chia J, Browne KA, Ciccone A, Ellis S, Lopez JA, *et al.* Protection from endogenous perforin: glycans and the C terminus regulate exocytic trafficking in cytotoxic lymphocytes. *Immunity* 2011, **34**(6): 879-892.

15. House IG, House CM, Brennan AJ, Gilan O, Dawson MA, Whisstock JC, *et al.* Regulation of perforin activation and pre-synaptic toxicity through C-terminal glycosylation. *EMBO Rep* 2017.

16. Voskoboinik I, Thia MC, Fletcher J, Ciccone A, Browne K, Smyth MJ, *et al.* Calcium-dependent plasma membrane binding and cell lysis by perforin are mediated through its C2 domain: A critical role for aspartate residues 429, 435, 483, and 485 but not 491. *J Biol Chem* 2005, **280**(9): 8426-8434.

17. Clementi R, Locatelli F, Dupre L, Garaventa A, Emmi L, Bregni M, *et al.* A proportion of patients with lymphoma may harbor mutations of the perforin gene. *Blood* 2005, **105**(11): 4424-4428.

18. Trambas C, Gallo F, Pende D, Marcenaro S, Moretta L, De Fusco C, *et al.* A single amino acid change, A91V, leads to conformational changes that can impair processing to the active form of perforin. *Blood* 2005, **106**(3): 932-937.

19. Voskoboinik I, Thia MC, Trapani JA. A functional analysis of the putative polymorphisms A91V and N252S and 22 missense perforin mutations associated with familial hemophagocytic lymphohistiocytosis. *Blood* 2005, **105**(12): 4700-4706.

20. Voskoboinik I, Sutton VR, Ciccone A, House CM, Chia J, Darcy PK, *et al.* Perforin activity and immune homeostasis: the common A91V polymorphism in perforin results in both presynaptic and postsynaptic defects in function. *Blood* 2007, **110**(4): 1184-1190.

21. Pankow S, Bamberger C, Calzolari D, Martinez-Bartolome S, Lavallee-Adam M, Balch WE, *et al.* F508 CFTR interactome remodelling promotes rescue of cystic fibrosis. *Nature* 2015, **528**(7583): 510-516.

22. Veit G, Avramescu RG, Chiang AN, Houck SA, Cai Z, Peters KW, *et al.* From CFTR biology toward combinatorial pharmacotherapy: expanded classification of cystic fibrosis mutations. *Mol Biol Cell* 2016, **27**(3): 424-433.

23. Voskoboinik I, Thia MC, De Bono A, Browne K, Cretney E, Jackson JT, *et al.* The functional basis for hemophagocytic lymphohistiocytosis in a patient with co-inherited missense mutations in the perforin (PFN1) gene. *The Journal of experimental medicine* 2004, **200**(6): 811-816.

24. Sutton VR, Waterhouse NJ, Baran K, Browne K, Voskoboinik I, Trapani JA. Measuring cell death mediated by cytotoxic lymphocytes or their granule effector molecules. *Methods* 2008, **44**(3): 241-249.

25. Kabsch W. Xds. *Acta Crystallogr D Biol Crystallogr* 2010, **66**(Pt 2): 125-132.

26. Evans PR. An introduction to data reduction: space-group determination, scaling and intensity statistics. *Acta Crystallogr D Biol Crystallogr* 2011, **67**(Pt 4): 282-292.

27. Winn MD, Ballard CC, Cowtan KD, Dodson EJ, Emsley P, Evans PR, *et al.* Overview of the CCP4 suite and current developments. *Acta Crystallogr D Biol Crystallogr* 2011, **67**(Pt 4): 235-242.

28. Evans PR, Murshudov GN. How good are my data and what is the resolution? *Acta Crystallogr D Biol Crystallogr* 2013, **69**(Pt 7): 1204-1214.

29. McCoy AJ, Grosse-Kunstleve RW, Adams PD, Winn MD, Storoni LC, Read RJ. Phaser crystallographic software. *J Appl Crystallogr* 2007, **40**(Pt 4): 658-674.

30. Emsley P, Lohkamp B, Scott WG, Cowtan K. Features and development of Coot. *Acta Crystallogr D Biol Crystallogr* 2010, **66**(Pt 4): 486-501.

31. Chen VB, Arendall WB, 3rd, Headd JJ, Keedy DA, Immormino RM, Kapral GJ, *et al.* MolProbity: all-atom structure validation for macromolecular crystallography. *Acta Crystallogr D Biol Crystallogr* 2010, **66**(Pt 1): 12-21.

Figure Legends

Figure 1: Ca^{2+}-dependent stabilisation of the C2 domain is necessary for efficient perforin folding and export from the ER.

(A) Western immunoblot demonstrates the relative perforin expression in each of the transiently transfected RBL cell populations (WT, D429A, D483A, D491A) in the presence of EndoH (+) or buffer only control (-). EndoH sensitive bands are highlighted by (*). The bar graph shows quantitative densitometry of the EndoH treated (+) protein lysates; mutation of essential Ca^{2+} binding residues causes a significant increase in % EndoH sensitive Prf1. EndoH sensitivity was calculated using the % EndoH cleaved protein versus the total amount of protein (cleaved and uncleaved) as detected by the PI-8 antibody. Shown is mean ± SEM of at least 3 independent experiments and statistics were determined using ANOVA and Tukey's post-hoc analysis, *$p < 0.05$.

(B) Western immunoblot using the P1-8 antibody demonstrates the relative perforin expression in RBL cells transiently transfected with WT and the W427A/Y430A/Y486A/W488A quadruple mutant (x4) in the presence of EndoH (EH), PNGaseF (PF) or buffer only control (Con); the EndoH sensitivity of the x4 Prf1 was indistinguishable from WT.

(C) Western immunoblot using the P1-8 antibody demonstrates the relative perforin expression in RBL cells transiently transfected with WT and the A90V mutant in the presence of EndoH (+) or buffer only control (-). EndoH sensitive bands are highlighted by (*). The bar graph shows quantitative densitometry of the EndoH treated (+) protein lysates; the mildly misfolded A90V Prf1 mutant caused a significant increase in % EndoH sensitive Prf1. EndoH sensitivity of WT and A90V perforin was calculated as described in Figure 1A. Shown is mean ± SEM of n=16 (WT) and n=7 (A90V) independent experiments and statistics were obtained with an unpaired two-sample for means t-test, *$p < 0.05$.

(D) Western immunoblot using the P1-8 antibody demonstrates the relative perforin expression in each of the transiently transfected RBL cell populations (WT, A90V/D429A, A90V/D483A, A90V/D491A) in the presence of EndoH (+) or buffer only control (-).EndoH sensitive bands are highlighted by (*). Shown is mean ± SEM of at least 3 independent experiments.

(E-G) Bar graphs showing quantitative densitometry of the EndoH treated (+) protein lysates from representative westerns in Figure 1C and 1D. To determine whether the double mutation of A90V and Ca^{2+} binding residues (A90V/D429A, A90V/D483A, A90V/D491A) had a synergistic effect on perforin stability and trafficking from the ER above normal background

levels, the % EndoH sensitive WT Prf1 was subtracted from the % EndoH sensitivity of perforin mutants. Dotted bars show predicted additive effect of individual mutants. Each value represents ± SEM for at least three independent experiments. The statistical significance was determined using ANOVA and Tukey's post-hoc analysis, *$p < 0.05$.

Figure 2: Prf1 protein is stabilized by a point mutation, T431D, in the C2 domain in the presence of Ca^{2+}.

(A) The thermal melting temperature of WT and mutant Prf1 in the presence of increasing Ca^{2+} concentrations: (left, WT and T431D Prf1) T431D Prf1 was significantly more stable than WT Prf1 in the presence of >1mM Ca^{2+}; (center, WT and D429A/T431D Prf1) inhibition of Ca^{2+} binding to the Prf1 C2 domain by D429A prevented any increase in T431D Prf1 thermal stability; (right, WT and A90V/T431D Prf1) the T431D mutation onto the backbone of A90V perforin resulted in greater thermal stability than WT perforin. Each value represents means ± SEM for three (left and center) or five (right) experiments, and statistics were obtained with an unpaired two-sample for means t test *$p < 0.05$.

(B) There was no significant difference in the lytic activity of recombinant WT and T431D Prf1 (left) and A90V/T431D Prf1 (right), as assessed using SRBCs.

(C) Western immunoblot using the P1-8 antibody demonstrates the relative Prf1 expression in each of the transiently transfected RBL cell populations (WT, T431D, A90V and A90V/T431D) in the presence of EndoH (+) or buffer only control (-). Endo H sensitive band is highlighted by (*). The bar graph shows densitometry analysis of the EndoH treated (+) protein lysates; the T431D mutation restored the % EndoH sensitivity of A90V to WT Prf1 levels (A90V/T431D). EndoH sensitivity of perforin was calculated as described in Figure 1. WT and A90V values (*dotted lines*) are reproduced from Figure 1C (WT, n=16, A90V, n=7); n=3 for T431D and A90V/T431D. Statistical significance was determined using ANOVA and Tukey's post-hoc analysis, *$p < 0.05$.

(D) Western immunoblot using the P1-8 antibody demonstrates the relative Prf1 expression in each of the transiently transfected RBL cell populations (WT, D429A/T431D, A90V/D429A/T431D) in the presence of EndoH (+) or buffer only control (-). The bar graph shows densitometry of the EndoH treated (+) protein lysates; T431D Prf1 did not restore the % EndoH sensitivity to WT levels in the presence of the D429A Ca^{2+} binding mutation. EndoH sensitivity of perforin was calculated as described in Figure 1A. D429A and A90V/D429A values

(*dotted lines*) are reproduced from Figure 1E. Each value represents ± SEM for at least three independent experiments and statistics were determined using ANOVA and Tukey's post-hoc analysis, *nsd:* no significant difference.

Figure 3. Crystal structure of T431 Prf1 reveals conformational changes in the Calcium Binding Regions (CBRs).

Superposition of C2 domains crystal structures. **A.** C2 domain of full-length perforin (PDB ID 3NJS, grey), C2_T431 (PDB IB 4Y1S, cyan, left) and C2_D431 (skyblue, right), No Ca2+ was added to the sample buffers or cyrstallization buffers (see *Materials and Methods*). Also shown are high affinity Ca2+ ions in the structures, presumably scavenged from the growth media, they are found in sites II and V of 3NJS, site V of C2_T431; no Ca2+ is found in the C2_D431 structure. All Ca2+ ions shown are coloured according to the corresponding C2 structures. Residues 433-438 of C2_T431 are missing from the electron density map and are represented as a red dashed line (left). **B.** Crystal structures of C2 domains C2_T431 (PDB ID 4Y1T, cyan, left and bottom) and C2_D431 (skyblue, right and bottom) obtained in the presence of added Ca2+. Also shown is the C2 domain of full-length perforin (PDB ID 3NJS, grey, left and right) as for A. The structure of C2_D431 reveals three Ca2+ ions (CaI-III), whereas five Ca2+ ions can be observed in the structure of C2_T431. Also shown are residues D429, D483, D491, CBR 1-3 and loop 510-515 and distances between CaI and D429 and D491 (in angstrom, red).

Figure 4: Stabilisation of Prf1 with T431D increased the rate of target cell lysis.

(A) Binding of recombinant WT and T431D perforin to SRBC membranes. There was no significant difference in the amount of T431D perforin bound to SRBC membranes in 1mM Ca^{2+}, or avidity of membrane binding, as detected by western blot after washing in Ca^{2+}-free buffer.

(B) Negative stain electron microscopy images of Prf1 oligomers on lipid monolayers. T431D oligomerises into arcs and rings similar to WT Prf1. Scale bar, 20 nm.

(C) Prf1/GrzmB synergy is not affected by stabilisation of Prf1 with T431D. HeLa cells were treated with sublytic Prf1 in the absence (Prf1 only) or presence of 2, 3 and 5 μg of GrzmB and a 4 h ^{51}Cr release assay was performed. Each value is ± SEM of three replicates, and is representative of 2 independent experiments. Statistics were obtained using unpaired t-test, *ns:* no significant difference.

(D) The rate of SRBC lysis was increased almost 2-fold by stabilisation of Prf1 with T431D. $5x10^8$

SRBCs/ml were incubated with purified recombinant mouse WT and T431D Prf1 in 1mM Ca^{2+} at 37°C. The SRBC/Prf1 reaction was quenched with ice-cold EDTA after 30 sec, 1, 2, 3, 4, 5, 10 and 15 mins. All values have been normalized against maximum lysis observed at 15 mins (100%); average maximum lysis was WT: 73.0 ± 10.0 SEM (n=7) and T431D: 74.6 ± 12.2 SEM (n=7). Dotted lines represent the time required to achieve 50% maximum cell lysis: 4.9±0.4min and 2.5±0.3min (mean±SEM, n=7 independent experiments; $p<0.0005$ unpaired t-test) for WT and T431D, respectively.

(E) The lytic activity of recombinant WT and T431D Prf1 (left) and A90V/T431D Prf1 (right) in the presence of increasing Ca^{2+} concentrations was assessed using SRBCs. At sub-physiological Ca^{2+} concentrations of <0.5mM, T431D and A90V/T431D had relatively lower cytotoxic activity than WT Prf1.

Figure 5: Stabilisation of Prf1 with T431D increases cellular cytotoxicity.

(A) Cytotoxicity of transiently transfected RBL cells expressing WT and T431D Prf1, as determined by ^{51}Cr release assay using Jurkat T-cells as targets, at the effector/target (E:T) ratios indicated (100% WT average maximum lysis at 30:1 E/T ratio was 42 ± 5 SEM). The data was fitted to Michaelis-Menten kinetics (using Prism 7.0.c). Using Michaelis-Menten equation, it was calculated that T431D required 4.9 effector cells (while WT required 30 effector cells) to achieve 100% lysis. Therefore, killer cells expressing T431D were 6.1-times more efficient than WT cells in producing an equivalent level of ^{51}Cr release (dotted lines). Each value represents mean ± SEM of three independent experiments.

(B) Cytotoxicity of transiently transfected RBL cells expressing WT and T431D Prf1 sorted for high and low GFP fluorescence, as determined by ^{51}Cr release assay using Jurkat T-cells as targets, at the effector/target (E:T) ratios indicated (100% WT average maximum lysis at 30:1 E/T ratio was 47.1 ± 11.5 SEM). The cytotoxicity of T431D was increased ~10-fold in low GFP expressing cells when compared with WT Prf1. Each value represents mean ± SEM of three independent experiments. Western immunoblot using the P1-8 antibody demonstrated equivalent protein expression of WT and T431D Prf1 in low and high GFP expressing RBL cells.

(C) Cytotoxicity of transiently transfected RBL cells expressing WT and T431D Prf1, at increasing concentrations of Ca^{2+}, as determined by a ^{51}Cr release assay using Jurkat T-cells as targets, at a constant effector target (E:T) ratio of 30:1. Ca^{2+} was quenched from DMEM media

using EGTA. Each value is mean ± SEM of three replicates, and is representative of 2 experiments.

(D) Cytotoxicity of transiently transfected RBL cells expressing WT, T431D, A90V and A90V/T431D Prf1, as determined by ^{51}Cr release assay using Jurkat T-cells as targets, at the effector/target (E:T) ratios indicated (100% WT average maximum lysis at 30:1 E/T ratio was 50 ± 6% SEM). The A90V/T431D Prf1 had ~5-fold increase in cytotoxicity when compared with the disease causing mutant, A90V, alone. Each value represents mean ± SEM of three independent experiments.

(E) Wild-type or mutant perforin was transiently transfected (by electroporation) into RBL cells, plated and grown for 90-240 minutes. At the time-points shown above the Western blot (on the left), the cells were harvested by trypsinisation and the lysates were treated with EndoH to determine a relative proportion of EndoH-resistant (upper bands) and EndoH sensitive (lower band) perforin. The migration of deglycosylated perforin was determined by treating the lysate from a sample collected at 240min with PNGaseF (shown as "F") on the Western blot. "UT" indicates an untreated lysate. The ratio of upper and lower bands was determined from three independent experiments; plotted is an acquisition of EndoH resistance over time (mean ± SEM).

Table 1. Data collection and refinement statistics*

	C2_T431D[1]	C2_T431D_Ca[2]
Data collection		
Space group	$P2_12_12_1$	$I121$
No mol/au	1	1
Cell dimensions		
a, *b*, *c* (Å)	27.77 66.03 74.9	51.00 31.31 86.36
α, β, γ (°)	90, 90, 90	90, 101.35, 90
Resolution (Å)	33.01 (2.00)	42.34 (1.80)
R_{merge} / R_{pim}	1.514 / 0.604	0.408 / 0.360
I/sI	2.6	2.5
Completeness (%)	100 (100)	99.3 (88.6)
Redundancy	7.0 (7.3)	4.1 (3.5)
Refinement		
No. reflections (work/free)	2591/115	2829/145
R_{work}/ R_{free}	19.1/22.2	21.1/23.3
No. atoms		
Protein	956	980
Ligand/ion	1	3
Water	70	90
B-factors		
Protein	30.21	30.21
Ligand/ion	19.28	18.99
Water	32.95	35.59
r.m.s deviations		
Bond lengths (Å)	0.010	0.010
Bond angles (°)	1.12	1.09
MolProbity analysis		
Ramachandran outliers	0%	0%
Ramachandran favoured	96.64%	93.14%
MolProbity score	100%	100%

*Highest resolution shell is shown in parenthesis.
[1]Structure consists of residues 410-427, 431-535.
[2]Structure consists of residues 410-535.

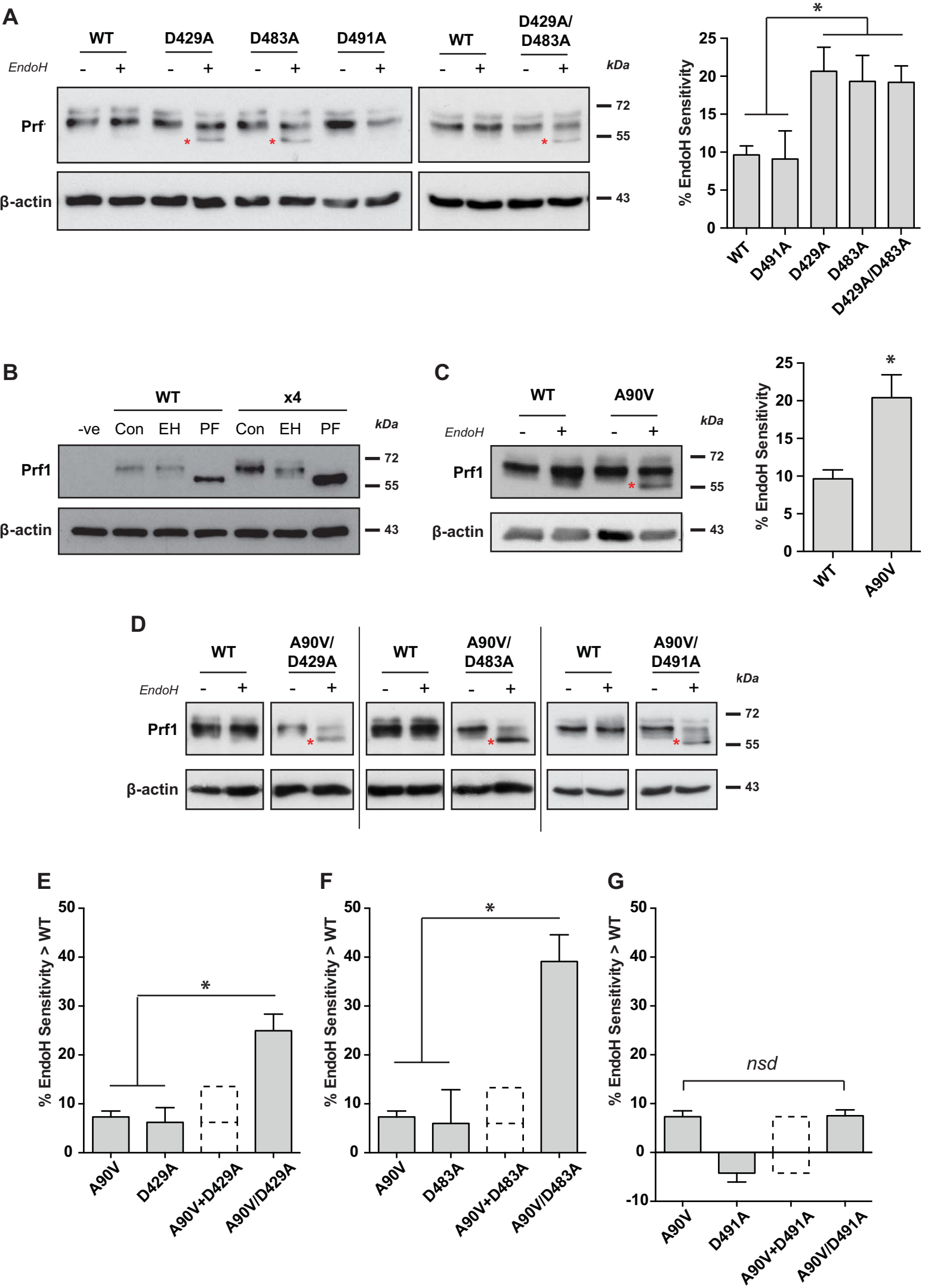
A
WT
D429A
D483A
D491A
WT
D429A/
D483A
EndoH
- + - + - + - + - + - +
kDa
Prf
β-actin
72
55
43
% EndoH Sensitivity
25
20
15
10
5
0
*
WT
D491A
D429A
D483A
D429A/D483A
B
WT
x4
-ve
Con
EH
PF
Con
EH
PF
kDa
Prf1
β-actin
72
55
43
C
WT
A90V
EndoH
- + - +
kDa
Prf1
β-actin
72
55
43
% EndoH Sensitivity
25
20
15
10
5
0
*
WT
A90V
D
WT
A90V/
D429A
WT
A90V/
D483A
WT
A90V/
D491A
EndoH
- + - + - + - + - + - +
kDa
Prf1
β-actin
72
55
43
E
% EndoH Sensitivity > WT
50
40
30
20
10
0
*
A90V
D429A
A90V+D429A
A90V/D429A
F
% EndoH Sensitivity > WT
50
40
30
20
10
0
*
A90V
D483A
A90V+D483A
A90V/D483A
G
% EndoH Sensitivity > WT
50
40
30
20
10
0
-10
nsd
A90V
D491A
A90V+D491A
A90V/D491A

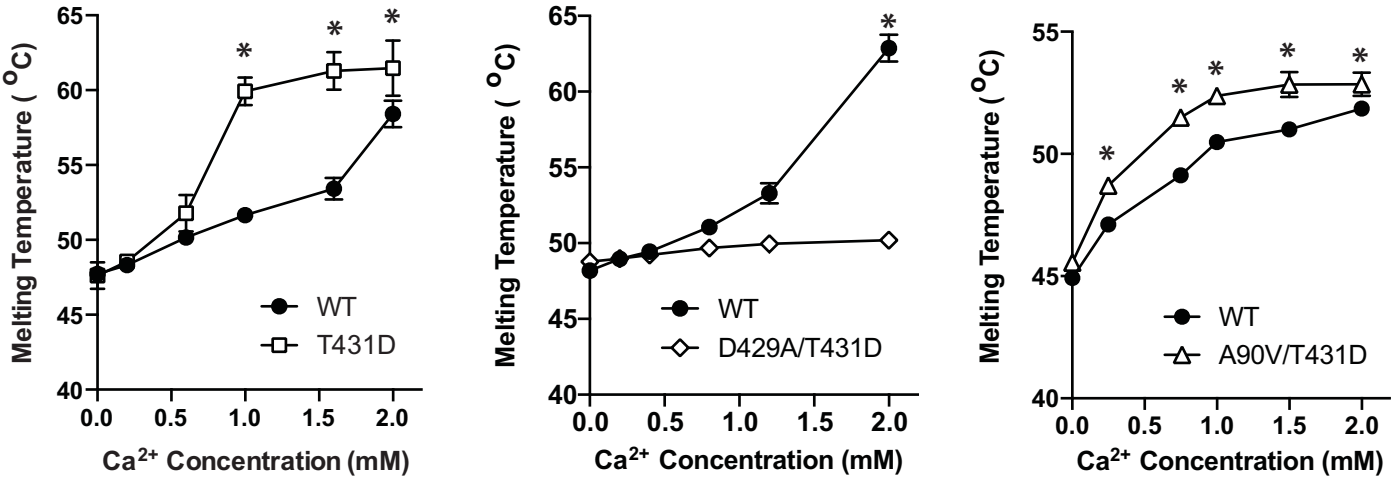
A
Melting Temperature (°C)
Ca2+ Concentration (mM)
WT
T431D
D429A/T431D
A90V/T431D

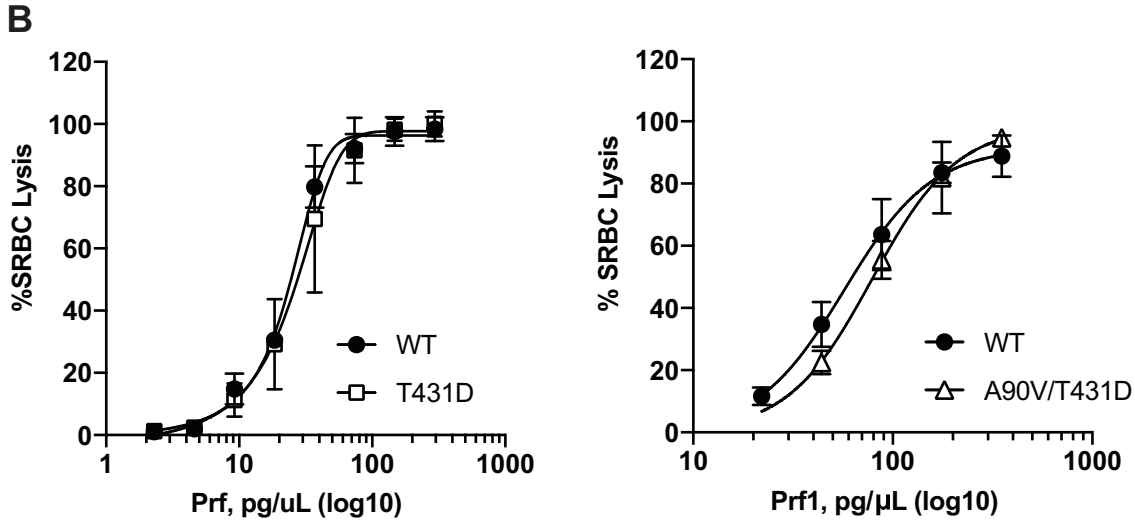
B
%SRBC Lysis
% SRBC Lysis
Prf, pg/uL (log10)
Prf1, pg/µL (log10)
WT
T431D
A90V/T431D

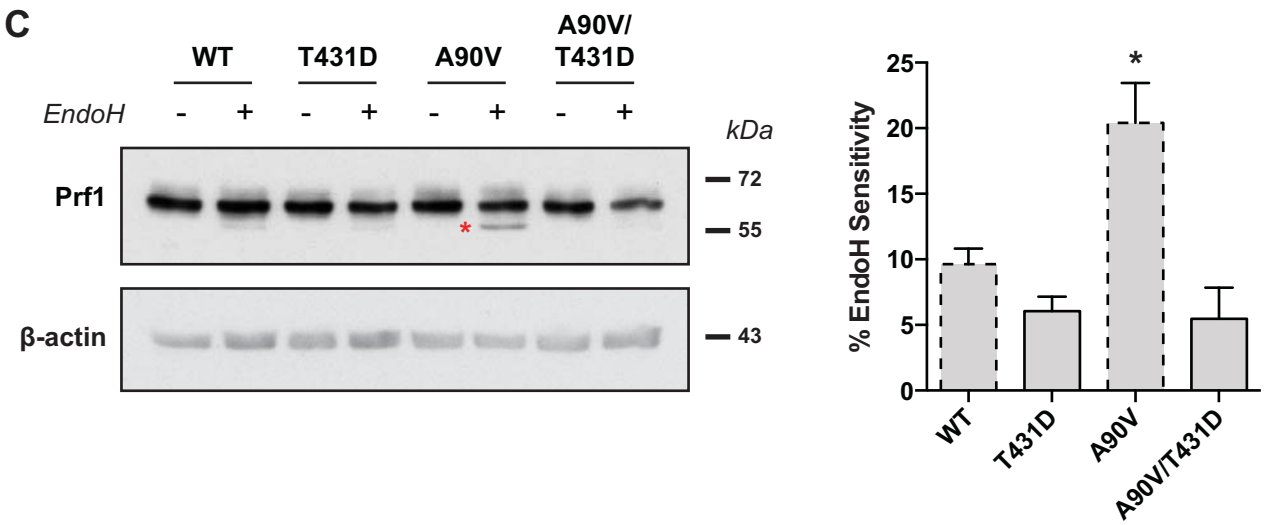
C
WT
T431D
A90V
A90V/
T431D
EndoH
kDa
Prf1
β-actin
72
55
43
% EndoH Sensitivity

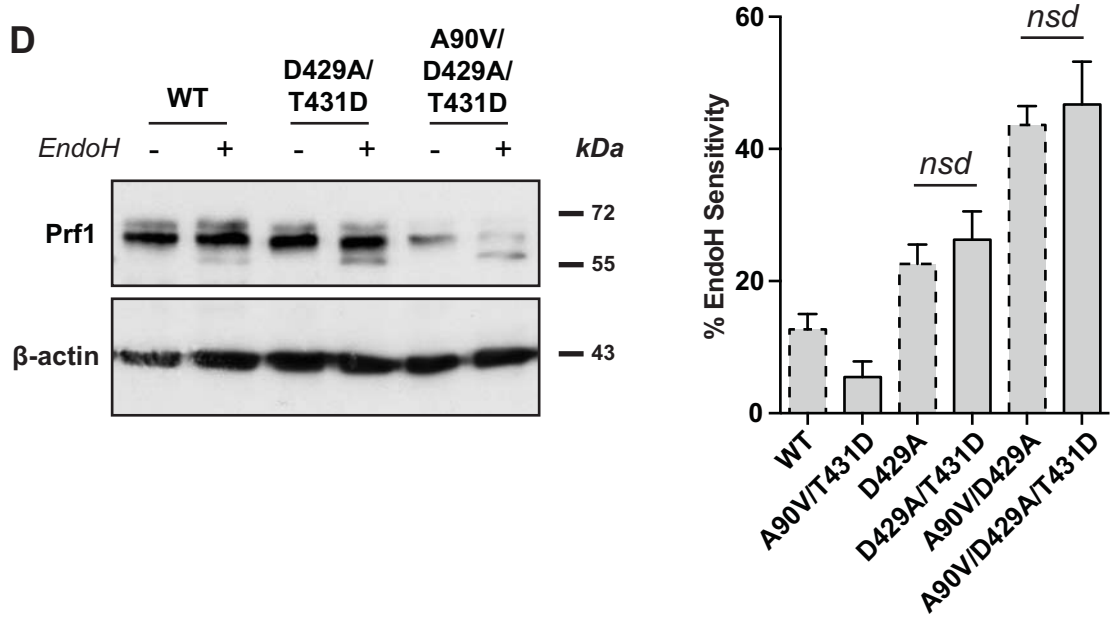
D
WT
D429A/
T431D
A90V/
D429A/
T431D
EndoH
kDa
Prf1
β-actin
72
55
43
% EndoH Sensitivity
nsd
WT
A90V/T431D
D429A
D429A/T431D
A90V/D429A
A90V/D429A/T431D

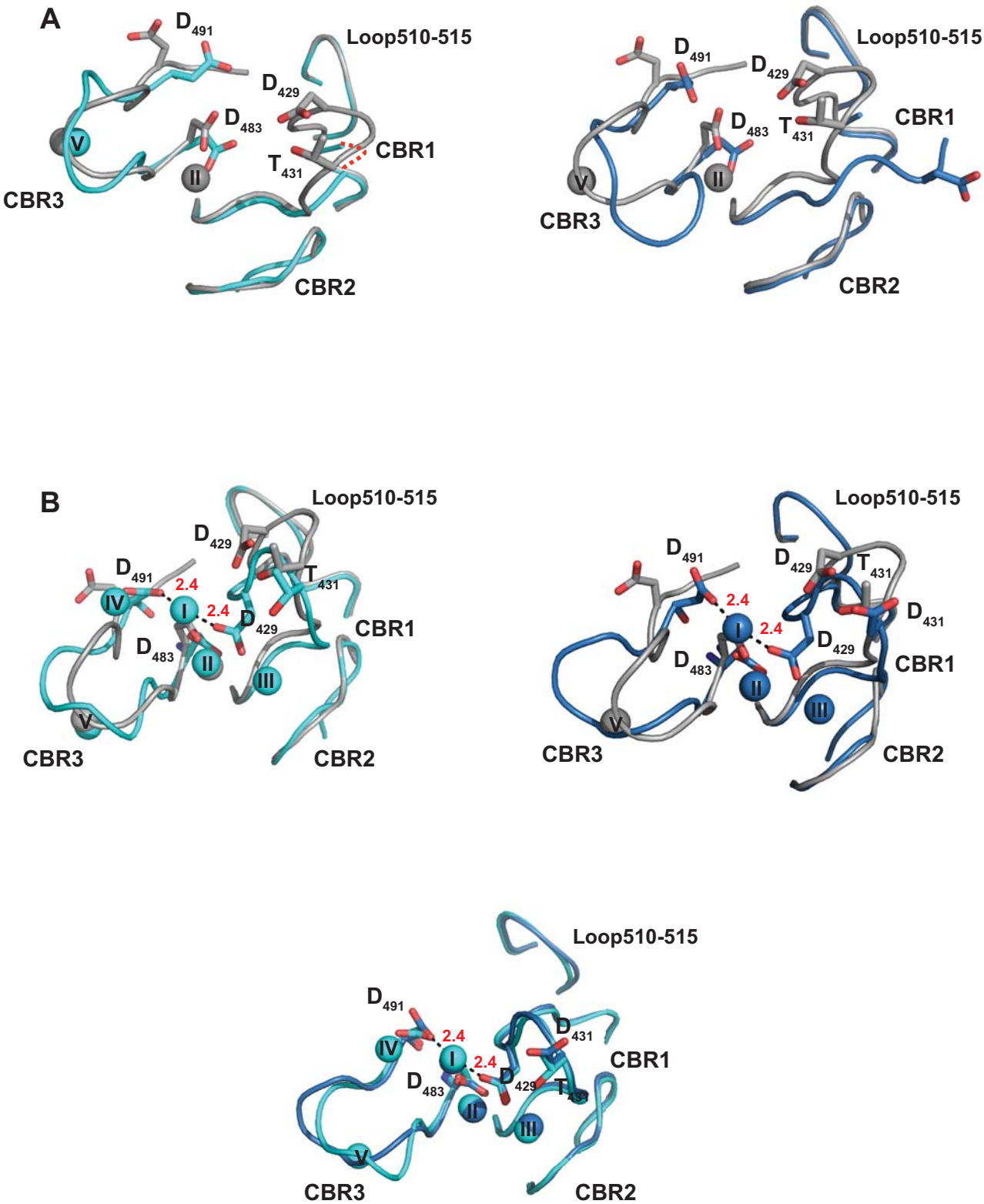
A
D491
Loop510-515
D429
D483
V
II
T431
CBR1
CBR3
CBR2
D491
D429
Loop510-515
D483
T431
CBR1
V
II
CBR3
CBR2
B
Loop510-515
D429
D491
T431
2.4
IV
I
2.4
D429
CBR1
D483
II
III
V
CBR3
CBR2
Loop510-515
D491
D429
T431
2.4
I
2.4
D431
D429
D483
CBR1
II
III
V
CBR3
CBR2
Loop510-515
D491
D431
2.4
IV
I
2.4
CBR1
D483
D429
II
III
V
CBR3
CBR2

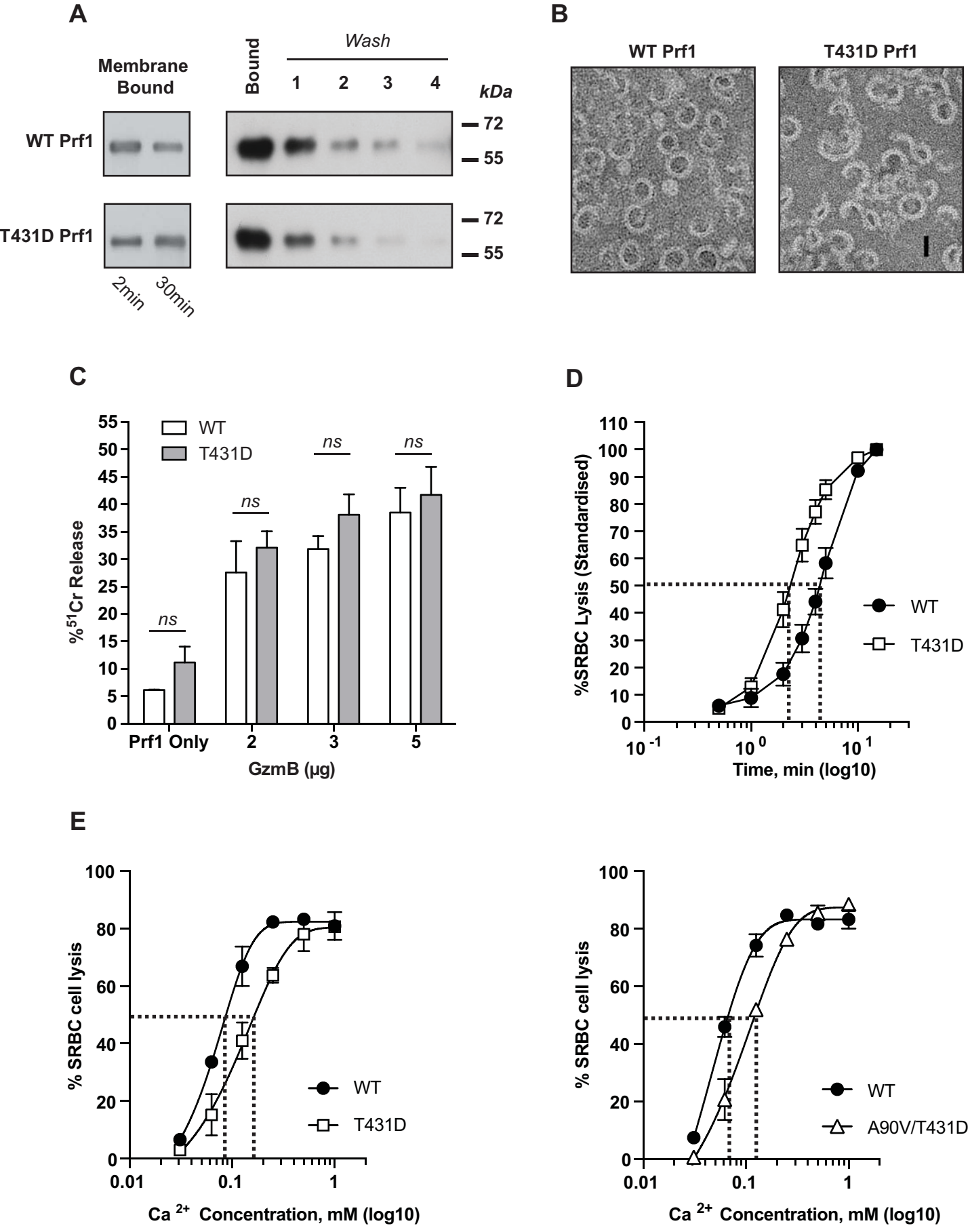
A
Membrane Bound
Bound
Wash
1
2
3
4
kDa
WT Prf1
T431D Prf1
72
55
72
55
2min
30min
B
WT Prf1
T431D Prf1
C
WT
T431D
ns
ns
ns
ns
%51Cr Release
Prf1 Only
2
3
5
GzmB (µg)
D
%SRBC Lysis (Standardised)
WT
T431D
Time, min (log10)
E
% SRBC cell lysis
WT
T431D
Ca 2+ Concentration, mM (log10)
% SRBC cell lysis
WT
A90V/T431D
Ca 2+ Concentration, mM (log10)

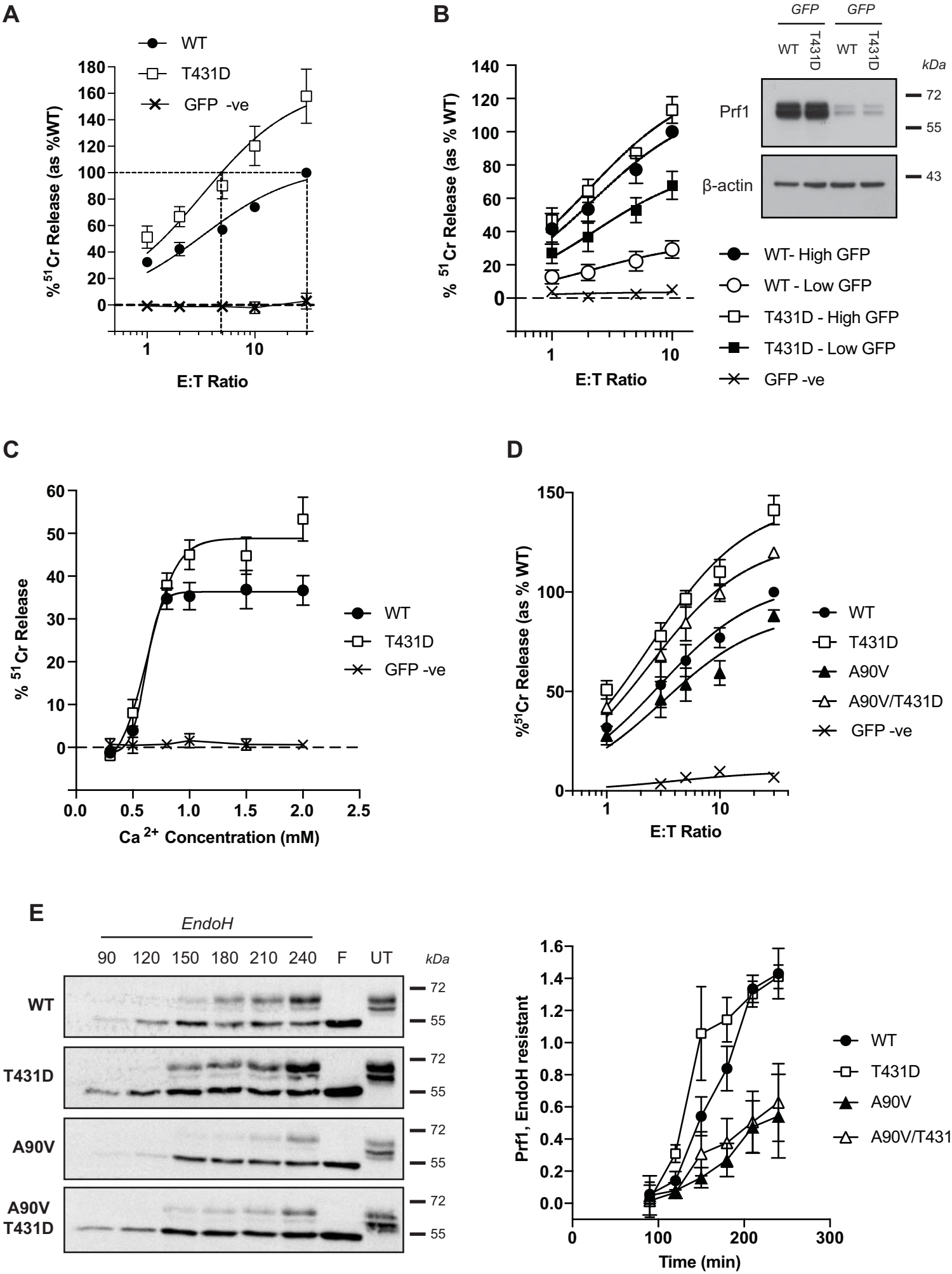
A
WT
T431D
GFP -ve
% 51Cr Release (as %WT)
E:T Ratio
B
HIGH GFP
LOW GFP
WT
T431D
WT
T431D
kDa
Prf1
β-actin
72
55
43
% 51Cr Release (as % WT)
E:T Ratio
WT- High GFP
WT - Low GFP
T431D - High GFP
T431D - Low GFP
GFP -ve
C
% 51Cr Release
Ca 2+ Concentration (mM)
WT
T431D
GFP -ve
D
%51Cr Release (as % WT)
E:T Ratio
WT
T431D
A90V
A90V/T431D
GFP -ve
E
EndoH
90 120 150 180 210 240 F UT
kDa
WT
T431D
A90V
A90V T431D
72
55
Prf1, EndoH resistant
Time (min)
WT
T431D
A90V
A90V/T431D